Oncogene (2017), 1–16

www.nature.com/onc

ORIGINAL ARTICLE

Metabolic inhibitors accentuate the anti-tumoral effect of HDAC5 inhibition

E Hendrick[1,10], P Peixoto[2,10], A Blomme[2], C Polese[1], N Matheus[1], J Cimino[3], A Frère[1,4], A Mouithys-Mickalad[5], D Serteyn[5], L Bettendorff[6], B Elmoualij[7], P De Tullio[8], G Eppe[9], F Dequiedt[1], V Castronovo[2] and D Mottet[1]

The US FDA approval of broad-spectrum histone deacetylase (HDAC) inhibitors has firmly laid the cancer community to explore HDAC inhibition as a therapeutic approach for cancer treatment. Hitting one HDAC member could yield clinical benefit but this required a complete understanding of the functions of the different HDAC members. Here we explored the consequences of specific HDAC5 inhibition in cancer cells. We demonstrated that HDAC5 inhibition induces an iron-dependent reactive oxygen species (ROS) production, ultimately leading to apoptotic cell death as well as mechanisms of mitochondria quality control (mitophagy and mitobiogenesis). Interestingly, adaptation of HDAC5-depleted cells to oxidative stress passes through reprogramming of metabolic pathways towards glucose and glutamine. Therefore, interference with both glucose and glutamine supply in HDAC5-inhibited cancer cells significantly increases apoptotic cell death and reduces tumour growth *in vivo;* providing insight into a valuable clinical strategy combining the selective inhibition of HDAC5 with various inhibitors of metabolism as a new therapy to kill cancer cells.

Oncogene advance online publication, 17 April 2017; doi:10.1038/onc.2017.103

INTRODUCTION

In oncology, histone deacetylases (HDAC) are considered as a promising class of anti-cancer targets. Eighteen HDAC members have been identified in human and grouped into four classes based on their sequence homology to their yeast *Saccharomyces cerevisiae* counterpart. Class I (HDAC1, 2, 3 and 8), Class II (subdivided into Class IIa HDAC4, 5, 7, and 9 and Class IIb HDAC6 and 10), Class III also called Sirtuin (SIRT 1 − 7) and class IV (HDAC11).[1] Class I, II and IV are sensitive to a large panel of pharmacological broad-spectrum HDACi. These unselective HDACi show promising anti-tumoral activity both *in vitro* and *in vivo*. Based on their potent anti-cancer effects, numerous HDACi are currently being tested in various human clinical trials.[2,3] Four HDACi—Suberoylanilide hydroxamic acid (SAHA, Vorinostat), Romidepsin (Depsipeptide, FK228, Istodax), Belinostat (PXD101, Beleodaq) and Panobinostat (LBH589, Farydak)—were US FDA-approved for the treatment of refractory or relapsed cutaneous T-cell lymphoma (CTCL),[4] peripheral T-cell lymphoma (PTCL)[5,6] and multiple myeloma,[7] validating the concept of HDAC inhibition to treat cancer patients.

Despite promising results in the treatment of haematological disorders, HDACi in monotherapy have very limited effects in solid tumours.[3,8] There is therefore a clear need to improve the efficacy of these drugs in clinic. One way for such improvement is the development of more specific inhibitors directed against individual HDAC. By targeting the most relevant HDAC members critically involved in tumour progression, it may be possible to greatly improve treatment efficiency with the additional advantage of removing certain toxicities that may be associated with the inhibition of multiple HDAC. Therefore, a better knowledge of the role and mechanisms of action of the individual HDAC is required to selectively target the best HDAC and significantly improve clinical benefit in cancer patients. We and others have investigated the function of Class IIa HDAC5 in cancer cells and found that its specific depletion by RNAi induced the growth arrest of cancer cells *in vitro* and decreased tumour growth *in vivo*.[9–13]

Besides investigations on the specific role of individual HDAC members in cancer biology, a deeper understanding of the molecular mechanisms underlying specific HDAC functions would be helpful for identifying biological processes that will help to set the future direction of new combinatory strategies with HDAC inhibitor. Here, we wished to gain a better insight into the molecular mechanisms underlying the specific inhibition of HDAC5 in cancer cells.

RESULTS

HDAC5 depletion modulates iron/ROS-related gene expression

To determine the function of HDAC5 in cancer cells, we performed a transcriptional analysis of HDAC5-depleted HeLa cells. The differentially expressed genes are listed in Supplementary Table 1. We noticed changes in mRNA whose functions are relevant to complex I mitochondrial activity (NDUFB5,

[1]University of Liege, GIGA-Molecular Biology of Diseases, Protein Signalisation and Interaction (PSI) Laboratory, Liège, Belgium; [2]University of Liege, GIGA-Cancer, Metastasis Research Laboratory (MRL), Liège, Belgium; [3]University of Liege, GIGA-Cancer, Laboratory of Tumor and Development Biology (LBTD), Liège, Belgium; [4]University of Liege, Laboratory of Pharmaceutical Technology and Biopharmacy (LTPB), Center for Interdisciplinary Research on Medicines (CIRM), Liège, Belgium; [5]University of Liege, Centre for Oxygen, R&D (CORD), Institute of Chemistry, Liège, Belgium; [6]University of Liege, GIGA-Signal Neurosciences, Laboratory of Pathological Aging and Epilepsy, Liège, Belgium; [7]University of Liege, Department of Human Histology-CRPP, Liège, Belgium; [8]University of Liege, Drug Research Center, Center for Interdisciplinary Research on Medicines (CIRM), Medicinal Chemistry Department, Liège, Belgium and [9]University of Liege, CART-LSM, Inorganic Analytical Chemistry, Chemistry Department, Liège, Belgium. Correspondence: Dr D Mottet, Protein Signalisation and Interaction Laboratory, GIGA, University of Liège, GIGA Building, B34, +2, B-4000 Liège, Belgium.
E-mail: dmottet@ulg.ac.be
[10]These authors contributed equally to this work.
Received 17 October 2016; revised 28 February 2017; accepted 1 March 2017

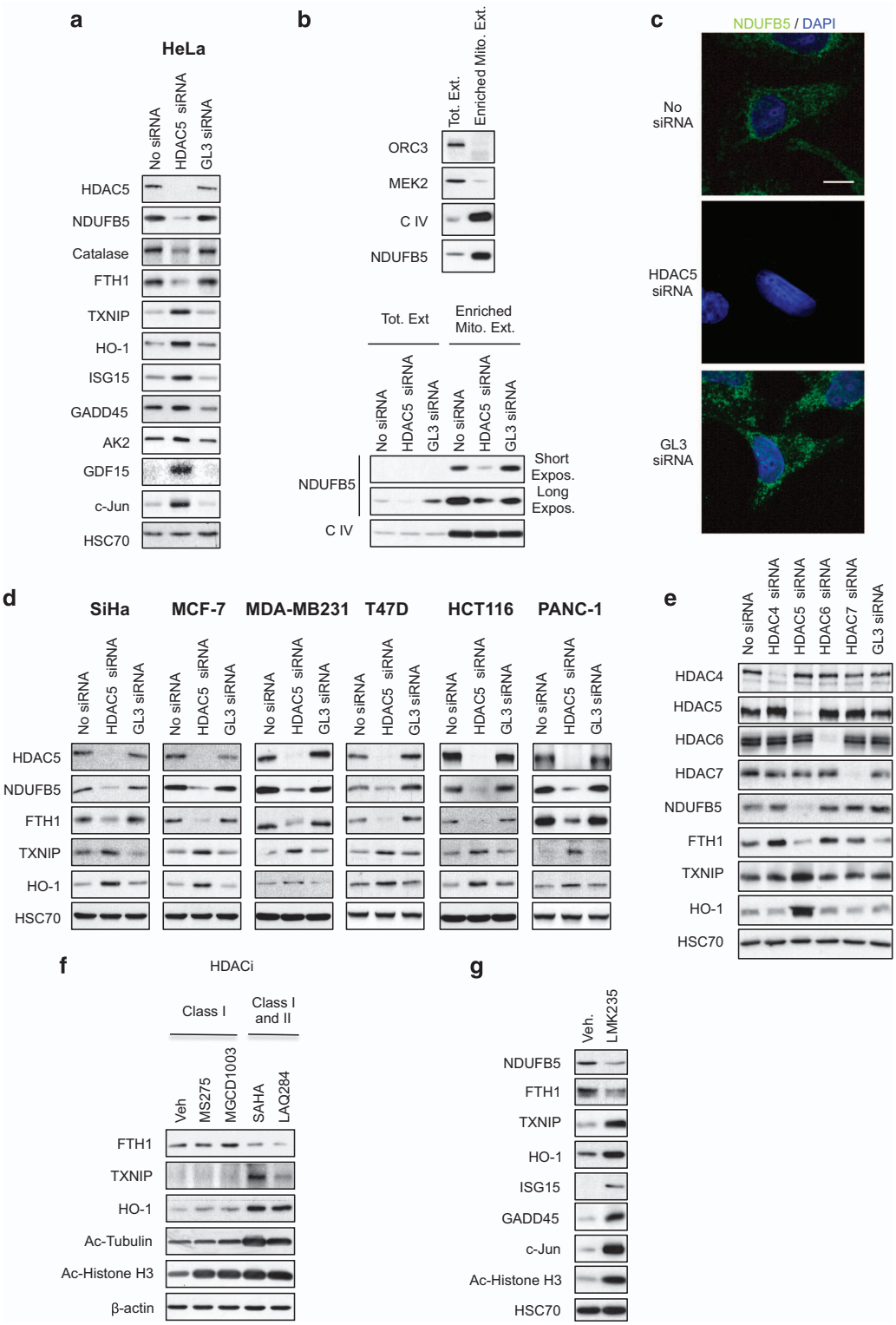

Figure 1. HDAC5 depletion modulates ROS-related gene expression. (**a**) Protein extracts from transfected HeLa cells were processed for immunoblot with indicated antibodies. (**b**) Fractions of mitochondrial-enriched proteins from transfected HeLa cells were prepared and immunoblots were performed with indicated antibodies. Fractions were controlled using MEK2 (cytoplasmic marker), ORC3 (nuclear/chromatin marker), NDUFB5 and mitochondrial complex IV subunit I (mitochondria marker). (**c**) The intracellular expression/localization of endogenous NDUFB5 protein in transfected HeLa cells was monitored by confocal immunofluorescence microscopy. (Magnification: ×630, Scale bar: 10 μm). (**d**) Different cancer cells (siHa, MCF-7, MDA-MB231, T47D, HCT116, PANC-1) were transfected with HDAC5 siRNA. Immunoblots were performed with indicated antibodies. (**e**) HeLa cells were transfected with siRNA directed against HDAC4, HDAC5, HDAC6 and HDAC7. Immunoblots were performed with indicated antibodies. (**f**) HeLa cells were treated with MS-275 (2 μM), MGCD1003 (2 μM), SAHA (2 μM) or LAQ824 (100 nM) for 24 h. Immunoblots were performed with indicated antibodies. (**g**) HeLa cells were treated with LMK235 (1 μM) for 24 h. Immunoblots were performed with indicated antibodies.

NDUFAB1, NDUFS4), reactive oxygen species (ROS) detoxifying enzymes (catalase, NQO1, GPX4 and GPX8, PDXK, HO-1) and many genes involved in the regulation of metal homeostasis, especially selenium (selenoprotein SELI, SELT), zinc (metallothionein MTE, MT1A, MT1E, MT2A) and iron metabolism (Ferritin FTH1, FTHL2, FTHL3, FTHL8, FTHL11, FTHL12, DMT1, CYBRD1, ISCA1, ISG15, SCARA5, IGFBP3, GDF15) (Figure 1 and– Supplementary Figures S1A – C). Validation experiments by RT-qPCR (Supplementary Figure S1D), western blot and immunofluorescence (Figures 1a–c) were conducted using several random target genes covering various fold change values. Transfection with a second HDAC5 siRNA had similar effects, excluding any off-target effect of HDAC5 siRNA (Supplementary Figures S1E – F). These protein modulations were also observed in other cell types, suggesting that the effect of HDAC5 silencing was not cell type-specific (Figure 1d). Among other class II HDAC, only HDAC5 silencing modulated those proteins (Figure 1e) showing the specific effect of HDAC5 depletion on gene modulation. Interestingly, class I/II HDACi (SAHA and LAQ824) but not class I-specific HDACi as well as the HDAC5 pharmacological inhibitor LMK235 showed similar effect than specific HDAC5 depletion with siRNA, suggesting that HDAC5 catalytic

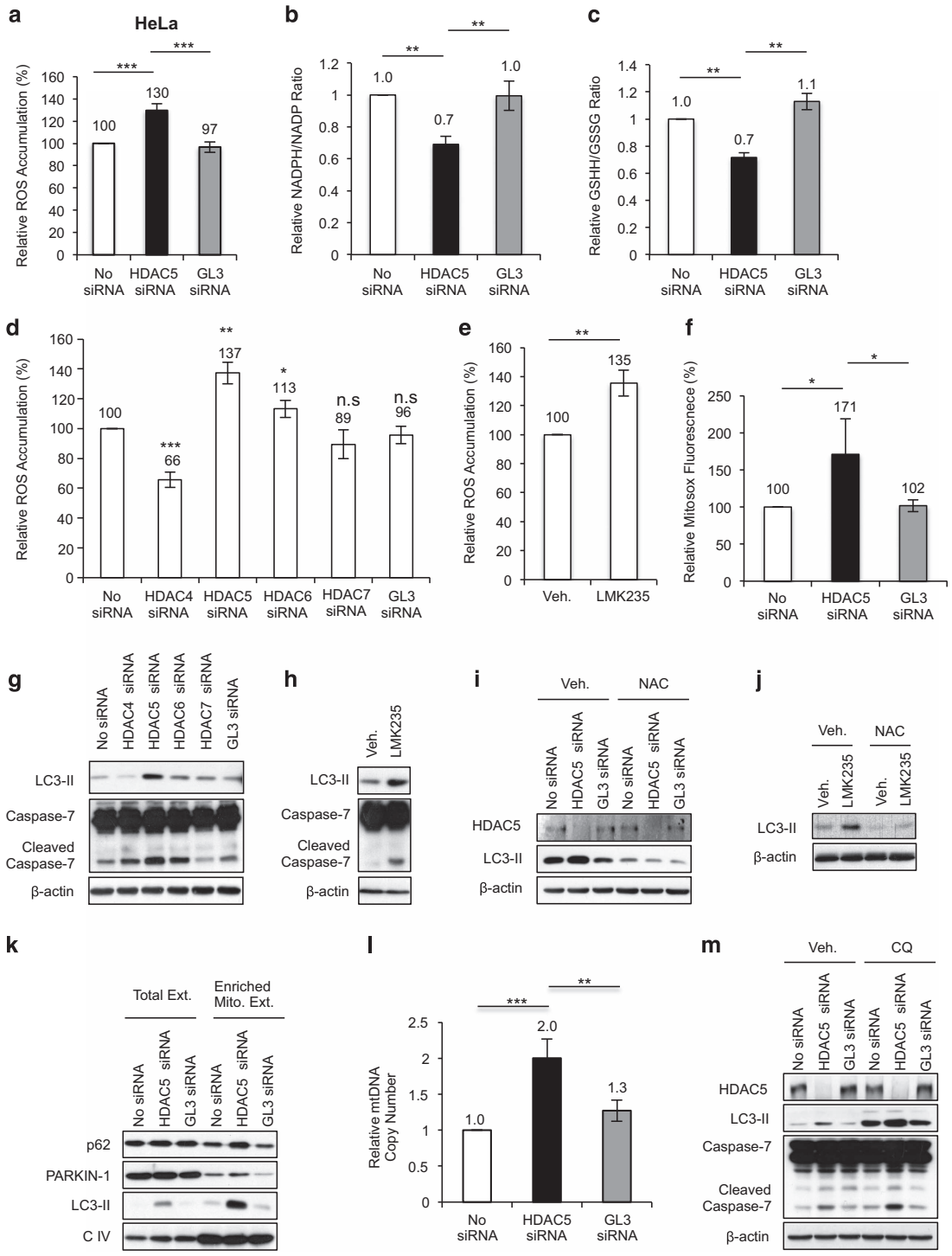

activity is required for modulation of gene expression profile (Figures 1f and g).

Oxidative stress upon HDAC5 depletion induces both apoptosis and autophagy

Because our transcriptomic analysis pointed towards an oxidative stress in HDAC5-depleted cells, we assessed the effect of HDAC5 depletion on ROS production. An increase in ROS production and low GSH/GSSG and NADPH/NADP ratios were observed in HDAC5-depleted cells (Figures 2a–c and Supplementary Figure S2), reflecting an oxidative stress. The depletion of other class II HDAC did not affect ROS except for HDAC6 (Figure 2d) while LMK235 also induced ROS accumulation (Figure 2e). As members of the mitochondrial complex I respiratory chain were modulated, we next determine whether the mitochondria were the main source of ROS. An increase in MitoSOX fluorescence intensity was measured in HDAC5-depleted cells suggesting that the detected ROS lie downstream of dismutated O_2^- derived from the mitochondrial chain (Figure 2f).

While ROS production leads to apoptosis, evidences demonstrate that low/transient ROS production can also induce autophagy.[14] Slight apoptosis as well as autophagy were induced upon HDAC5 depletion/inhibition compared to silencing of the other class II HDAC (Figures 2g and h and Supplementary Figures S3A–D). This was not observed in normal fibroblasts (Supplementary Figure S3E) or endothelial cells depleted for HDAC5 (data not shown,[15]). Autophagy induction upon HDAC5 depletion/inhibition was attributed to induction of ROS, as it was prevented by ROS scavenger *N*-acetyl-L-cysteine (NAC) (Figures 2i and j). With published electron microscopy analysis showing presence of mitochondria engulfed in autophagosomes,[9] we hypothesized that ROS-producing mitochondria were selectively degraded by a specific autophagic process called mitophagy.[16] Parkin, p62 and LC3 proteins in the mitochondria-enriched fraction were more abundant in HDAC5-depleted cells (Figure 2k), suggesting a higher mitophagy flux in these cells. As the removal of damaged mitochondria must be compensated by mitochondrial biogenesis to meet energy needs, we also observed a higher total mitochondrial DNA content in HDAC5-depleted cells (Figure 2l), demonstrating that HDAC5 depletion is also associated with mitochondrial biogenesis. Interestingly, when HDAC5 depletion was combined with chloroquine or bafilomycin A1, two autophagy inhibitors, apoptosis was increased, suggesting that autophagy acts as a survival mechanism (Figure 2m and Supplementary Figure S3F).

Alteration of iron homeostasis modulates oxidative stress and cell death of HDAC5-depleted cells

Under normal conditions, iron availability is regulated by sequestration. Indeed, ferritin can bind and sequester labile iron pool, limiting its availabilty for Fenton's reaction. Therefore, misregulation of iron homeostasis results in increased oxidative stress due to ROS generation. Several proteins known for their role in iron transport and storage were downregulated in HDAC5-depleted cancer cells. As expected, the intracellular iron level as well as the intracellular labile ferrous iron pool are increased upon HDAC5 depletion (Figures 3a and b).

Next, we assessed the sensitivity of HDAC5-depleted/inhibited cells to this iron dysregulation. Addition of deferoxamine (DFO), an iron chelator, decreased ROS levels (Figure 3c) and blocked cell death upon HDAC5 depletion (Figure 3d) while ferrous iron (Fe^{2+}) had the opposite effect (Figure 3e). These effects were less dramatically observed upon HDAC6 depletion (Supplementary Figure S4A). Interestingly, iron dysregulation modulated the accumulation of ROS and cell death upon LMK235 (Figures 3f – h) or SAHA treatment (Supplementary Figures S4B – D). Finally, since we previuously reported that HDAC5 depletion potentiates the effect of chemotherapeutic agents such as cisplatin[9] and there are indications in the literature that iron can influence cisplatin toxicity,[17,18] we examined the role of iron in cisplatin-induced cell death upon HDAC5 depletion. Apoptosis of HDAC5-depleted cells co-treated with cisplatin was blocked after addition of NAC, suggesting that cisplatin-induced apoptosis upon HDAC5 depletion is associated with oxidative stress (Figure 3i). We also demonstrated that this cytotoxicity of cisplatin in HDAC5-depleted cells relied on the presence of iron (Figures 3j and k), supporting evidences that iron supply might be required for therapies combining HDAC5 inhibition and cisplatin-induced oxidative stress.

HDAC5 depletion induces uncoupling mitochondrial respiration

The maintenance of an effective antioxidant defense system against ROS often results from changes in normal glucose and glutamine metabolism.[19] As both glucose and glutamine drive mitochondrial activity, we evaluated how HDAC5 depletion impacted on mitochondrial respiration. Routine respiration and proton leakage were increased in HDAC5-depleted cells compared with control cells (Figure 4a). A slight decrease in tetramethylrhodamine ethyl ester (TMRE) incorporation suggesting a small decrease in the mitochondrial membrane potential (mild uncoupling) but a constant total ATP level and a well-preserved energetic charge were observed upon HDAC5 depletion (Figures 4b–d). Together, these data suggest that HDAC5 depletion induces mild uncoupling

Figure 2. Oxidative stress upon HDAC5 depletion induces both apoptosis and autophagy. (**a**) ROS production in transfected HeLa cells was quantified using DCFDA dye (5 μM) and flow cytometry. Results are expressed in relative values (%) in reference to No siRNA condition taken as 100%. Data are mean ± s.d. of four independent experiments carried out in triplicate. (**b**) NADPH/NADP ratio measured in transfected HeLa cells. Results are presented as a relative ratio NADPH/NADP arbitrarily fixed as 1 in No siRNA condition. Values represented the mean ± s.d. of three independent experiments. (**c**) Measure of both reduced (GSG) and oxidized glutathione (GSSG) level in transfected HeLa cells cultured in high glucose medium for 24 h. Results are presented as a relative ratio GSH/GSSG arbitrarily fixed as 1 in No siRNA condition. Values represented the mean ± s.d. of three independent experiments. (**d**) HeLa cells were transfected with siRNA directed against HDAC4, HDAC5, HDAC6 and HDAC7. ROS production was quantified using DCFDA dye (5 μM) and flow cytometry. Results are expressed as in (**a**). Values represented the mean ± s.d. of four independent experiments. (**e**) HeLa cells were treated with LMK235 (1 μM). ROS production was quantified using DCFDA dye (5 μM) and flow cytometry. Results are expressed as in (**a**). Values represented the mean ± s.d. of four independent experiments carried out in triplicate. (**f**) Mitochondrial ROS production in transfected HeLa cells was quantified using Mitosox dye (5 μM) and flow cytometry. Results are expressed in relative values (%) in reference to No siRNA condition taken as 100%. Data are mean ± s.d. of three independent experiments carried out in triplicate. (**g**) HeLa cells were transfected with siRNA directed against HDAC4, HDAC5, HDAC6 and HDAC7. Immunoblots were performed with indicated antibodies. (**h**) HeLa cells were treated with LMK235 (1 μM). Immunoblots were performed with indicated antibodies. (**i**) Transfected HeLa cells were treated for additional 24 h in presence or absence of NAC (15 mM). Immunoblots were performed with indicated antibodies. (**j**) HeLa cells were treated with LMK235 (1 μM) in presence of NAC (15 mM). Immunoblots were performed with indicated antibodies. (**k**) Fraction of mitochondrial-enriched proteins were prepared from transfected HeLa cells. Immunoblots were performed with indicated antibodies. (**l**) Quantification of mitochondrial DNA copy number in transfected HeLa cells was measured. (**m**) Transfected HeLa cells were treated for additional 24 h in presence or absence of chloroquine (CQ–40 μM). Immunoblots were performed with indicated antibodies.

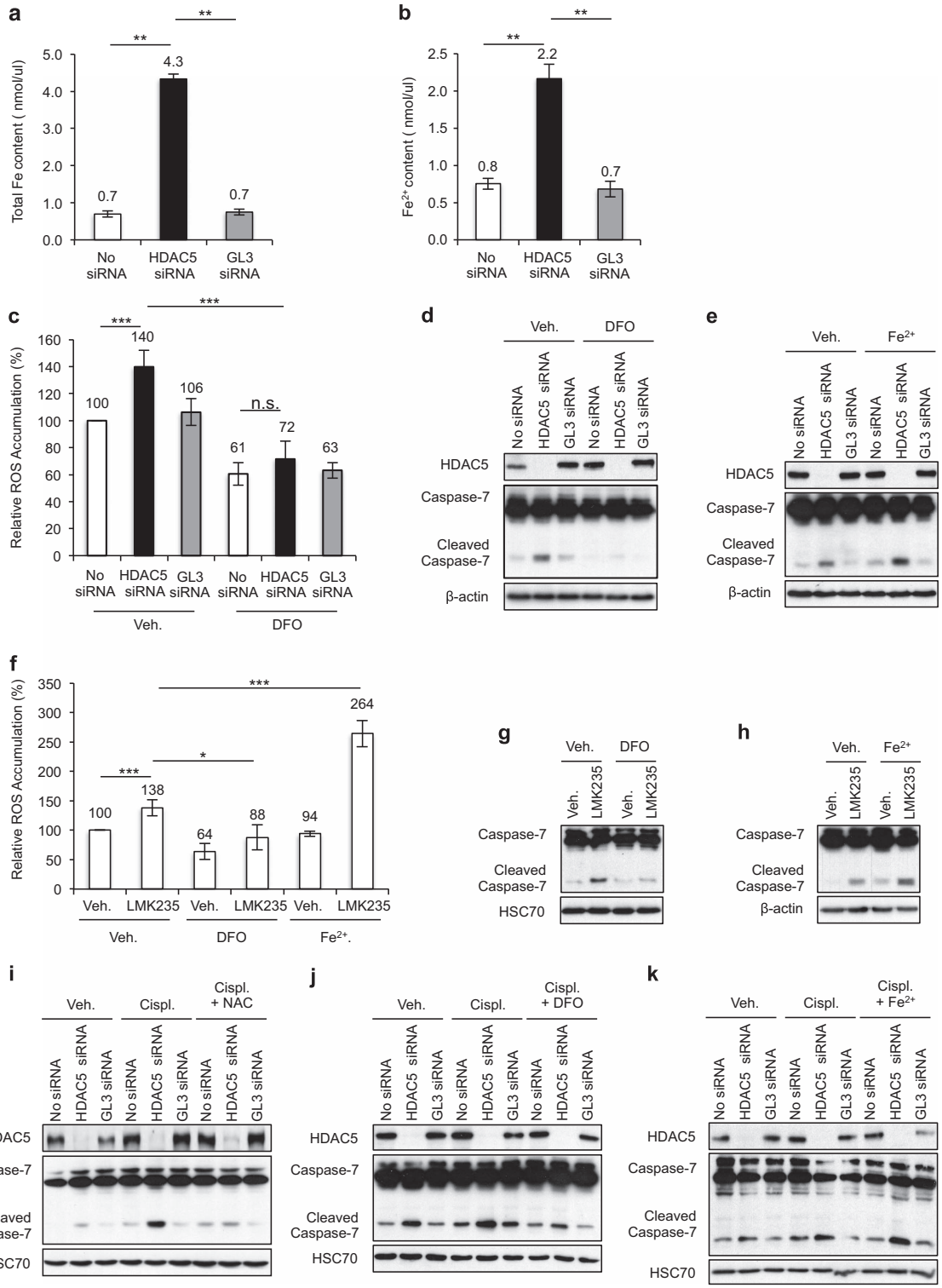

Figure 3. Alteration of iron level modulates oxidative stress and cell death of HDAC5-depleted cells. (**a**, **b**) Measure of both intracellular total iron (**a**) and ferrous iron (**b**) levels in transfected HeLa cells. Results are expressed in nmol/ul for 2×10^6 cells. Values represented the mean ± s.d. of three independent experiments. (**c**) ROS production in transfected HeLa cells co-treated with DFO (200 μM). Results are expressed as in Figure 2a. Values represented the mean ± s.d. of four independent experiments. (**d**, **e**) Transfected HeLa cells were treated either with DFO (200 μM) (**d**) or ferrous sulfate (Fe^{2+}–200 μM). (**e**) Immunoblots were performed with indicated antibodies. (**f**) ROS production in LMK235 (1 μM)-treated HeLa cells co-treated with DFO (200 μM). Results are expressed as in Figure 2a. Values represented the mean ± s.d. of three independent experiments. (**g**, **h**) LMK235 (1 μM)-treated HeLa cells were co-treated either with DFO (200 μM) (**g**) or ferrous sulfate (Fe^{2+}–200 μM) (**h**). Immunoblots were performed with indicated antibodies. (**i**–**k**) Transfected HeLa cells were treated with cisplatin (Cispl–5 μM) for additional 24 h in presence or absence of NAC (15 mM)) (**i**), DFO (200 μM) (**j**) or ferrous sulfate (Fe^{2+}–200 μM) (**k**). Immunoblots were performed with indicated antibodies.

respiration, a process that allows protons to flow across the mitochondrial membrane without producing any ATP.

Because mild mitochondrial uncoupling is a highly effective mechanism that can act as a modulator of oxidative stress and allow Krebs cycle to be kept functional to meet the biosynthetic demand,[20] we next assessed if mitochondrial respiration was required to moderate ROS production in HDAC5-depleted cells. Respiratory inhibitors (Rotenone and Antimycin A) allowed a larger generation of ROS (Figures 4e and f) and consequently accentuated cell death (Figures 4g – i), suggesting that the setting up of uncoupling respiration in HDAC5-depleted cells is an essential mechanism to moderate ROS production and control cell survival.

Reliance of HDAC5-depleted cells on PPP for cell survival

It is known that cancer cells require glucose metabolism. The first rate-limiting step of glucose metabolism is the transport of glucose across the plasma membrane. As predicted by our

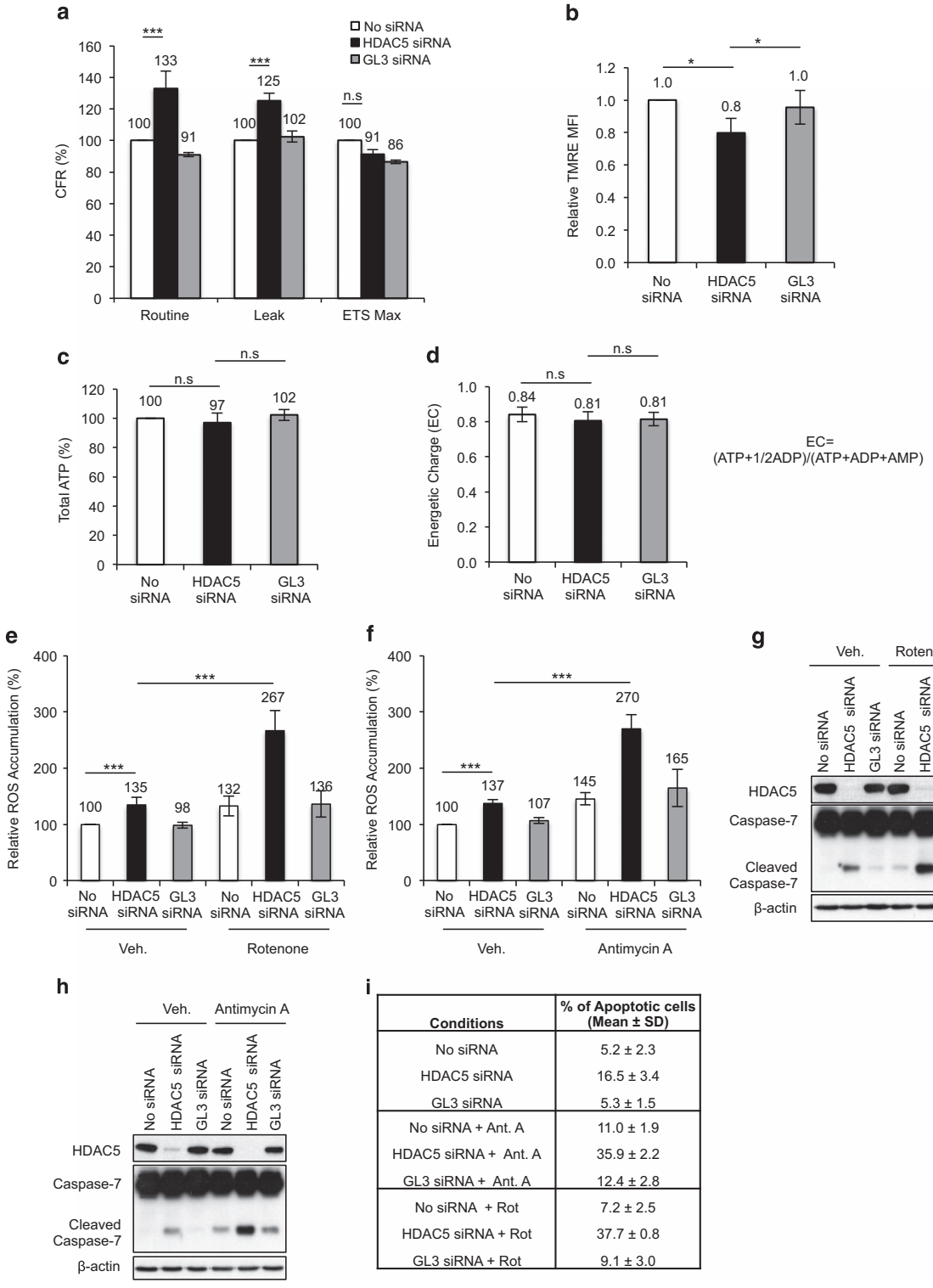

i

Conditions	% of Apoptotic cells (Mean ± SD)
No siRNA	5.2 ± 2.3
HDAC5 siRNA	16.5 ± 3.4
GL3 siRNA	5.3 ± 1.5
No siRNA + Ant. A	11.0 ± 1.9
HDAC5 siRNA + Ant. A	35.9 ± 2.2
GL3 siRNA + Ant. A	12.4 ± 2.8
No siRNA + Rot	7.2 ± 2.5
HDAC5 siRNA + Rot	37.7 ± 0.8
GL3 siRNA + Rot	9.1 ± 3.0

transcriptomic analysis, the high-affinity glucose transporter GLUT3 is increased in HDAC5-depleted cells (Supplementary Figure S1D) and an increase in glucose uptake is observed (Figure 5a).

Glucose can be metabolized by glycolysis, a catabolic process driven by the activation of enzymes leading to lactate production. Extracellular accumulation of lactate was unchanged (Figure 5b) and the expression levels of several key glycolytic enzymes were not altered (Figure 5c), suggesting that HDAC5 depletion did not directly increase glycolytic activity. Metabolized glucose can also converge towards the pentose phosphate pathway (PPP), a catabolic pathway that is considered as the major source of NADPH, a key reductive power for biosynthesis and redox balance. As HDAC5 depletion increased expression of both TIGAR and FBP-1 (Supplementary Figure S1D), two enzymes that are known to redirect carbon flux through the PPP, we hypothesized that survival of HDAC5-depleted cells relies on PPP. 6AN (an FDA-approved inhibitor of glucose-6-phosphate dehydrogenase) treatment combined with HDAC5 inhibition increased apoptotic cell death. Like 6AN, interference of G6PD expression using siRNA also increased apoptosis of HDAC5-depleted cells (Figures 5d–g). To determine the cause of 6AN cytotoxicity, levels of antioxidant molecules NADPH and GSH were measured. The NADPH/NADP and GSH/GSSG ratio declined upon HDAC5 depletion (Figures 5h and i) suggesting that NADPH supply was not sufficient for restoration of GSH and is consequently responsible for the production of highly cytotoxic ROS observed in HDAC5-depleted cells treated with 6AN (Figures 5j and k).

Glucose withdrawal-induced apoptotic cell death in HDAC5-depleted cancer cells is caused by oxidative stress

To further determine the importance of glucose in HDAC5-depleted cells, we cultured them in low glucose medium. The HDAC5-depleted cells were more susceptible to glucose deprivation-induced cell death than controls (Figures 6a–c). ATP levels were sustained in HDAC5-depleted cells cultured in low glucose medium (Figure 6d), indicating that upon HDAC5 silencing ATP depletion does not underlie the apoptosis. However, accumulation of ROS was observed in HDAC5-depleted cells cultured in low glucose medium (Figure 6e), which also displayed a compromised redox status evident from decreased GSH/GSSG and NADPH/ NADP ratios (Figures 6f and g). The administration of the antioxidant NAC upon glucose deprivation diminished cell death validating that ROS production is the cause of the apoptotic cell death (Figure 6h). Because it is not possible to totally deplete cancer cells of glucose *in vivo*, we have tested the effect of 2-DG, a relatively non-toxic analogue of glucose actually tested in clinic,[21,22] which creates a chemically induced state of glucose deprivation. Combination of 2-DG with HDAC5 depletion/inhibition increased cell death *in vitro* (Figures 7a–c). Because 2-DG can reduce the output from PPP (decrease NADPH production) and glycolysis/mitochondrial respiration (ATP), we next determine if oxidative and/or ATP stress could be contributing to 2-DG-induced cell death of HDAC5-depleted cells. ROS accumulation was further increased in HDAC5-depleted cells treated with 2-DG (Figure 7d). We also observed that 2-DG reduced ATP levels in HDAC5-depleted cells (Figure 7e). However, as co-incubation with NAC almost completely reversed 2-DG-induced apoptosis seen in cells depleted for HDAC5 (Figure 7f), this suggests that oxidative stress (not ATP stress) induced by glucose interference using 2-DG was the primary cause of apoptosis in HDAC5-depleted HeLa cells. The 2-DG-induced decrease in ATP levels would be directly linked to a decrease in mitochondrial activity, which would consequently induce a larger generation of ROS similarly as we observed using respiratory inhibitors in Figures 4e and f. Finally, the relevance of combining HDAC5 depletion and 2-DG *in vivo* was addressed using tumour mouse model. As expected, the combined treatment reduces tumour growth compared to single treatment, underlying the potential interest of such treatment in cancer therapy (Figures 7g and h).

Increased contribution of glutamine to the TCA cycle through oxidative metabolism in HDAC5-depleted cells.

Similarly to glucose, glutamine is a key nutrient that participates in redox homeostasis and macromolecular synthesis. To determine the glutamine dependency of HDAC5-depleted cells for survival, we cultured them in absence of glutamine. Glutamine deprivation further increased apoptosis of HDAC5-depleted cells (Figure 8a). To gain a better insight on the flux of glutamine upon HDAC5 depletion, transfected cells were incubated with fully labelled [U-^{13}C]-glutamine and analysed by GC-MS. In absence of HDAC5, cells displayed an increase in m+5 glutamine and m+5 glutamate, which predominantly fuels tricarboxylic acid (TCA) cycle or Krebs cycle flux as illustrated by higher fraction of m+4 citrate, m+4 malate, m+4 fumarate and m+4 succinate (Figures 8b and c), suggesting that HDAC5-depleted cells upregulates, at least, oxidative phosphorylation driven by glutamine.

Glutamine withdrawal-induced apoptotic cell death in HDAC5-depleted cancer cells through an energetic stress

To further explore the importance of HDAC5-depleted cells on glutamine for cell survival, we treated them with glutamine-interfering molecules. GPNA (glutamine transporter inhibitor) and BPTES (glutaminase synthase inhibitor) dramatically increased cell death (Figures 8d and e). Similarly, the combination of EGCG (glutamate dehydrogenase inhibitor) or AOA (aminotransferase inhibitor) and HDAC5 depletion caused a significant increase in cell death, suggesting that HDAC5-depleted cells require both GLUD1 and transaminases for cell survival (Figures 8f – h). Interestingly, exposing glutamine-deprived HDAC5-depleted cells to cell permeable dimethyl-α-ketoglutarate (DMK) alone did not rescue cell death upon glutamine deprivation. However, we found that supplementation with DMK and aspartate can reverse death

Figure 4. HDAC5 depletion induces uncoupling respiration. (**a**) Basal, uncoupled and maximal oxygen consumption rate was assessed in transfected HeLa cells 24 h post-transfection. Results are presented as relative values arbitrarily fixed as 100% in No siRNA condition. Data are mean ± s.d. of three independent experiments carried out in triplicate. (**b**) Mitochondrial membrane potential in transfected HeLa cells was assessed by TMRE mean fluorescence intensity, corrected by FCCP. Results are presented as relative values arbitrarily fixed as 1 in No siRNA condition. Data are mean ± s.d. of three independent experiments carried out in triplicate. (**c**) Measure of total ATP levels in transfected HeLa cells cultured in high glucose medium for 24 h. Results are presented as relative values arbitrarily fixed as 100% in No siRNA condition. Data are mean ± s.d. of three independent experiments carried out in triplicate. (**d**) Values for energy charge were calculated from the concentrations of adenine-derived nucleotides in transfected HeLa cells measured by HPLC according to the indicated formula. Data are mean ± s.d. of three independent experiments carried out in triplicate. (**e**, **f**) ROS production in transfected HeLa cells co-treated with rotenone (100 nM) (**e**) or antimycin A (1 μM) (**f**). Results are expressed as in Figure 2a. Values represented the mean ± s.d. of four independent experiments. (**g**, **h**) Transfected HeLa cells were treated either with rotenone (100 nM) (**g**) or antimycin A (1 μM) (**h**). Immunoblots were performed with indicated antibodies. (**i**) Quantification of apoptosis of transfected HeLa cells co-treated with rotenone (100 nM) or antimycin A (1 μM). Values represented the mean ± s.d. of three independent experiments.

of HDAC5-depleted cells (Figure 8i), suggesting that the alpha-ketoglutarate/aspartate metabolism is crucial to support cell survival.

Next, we determined how glutamine deprivation was responsible for the cell death of HDAC5-depleted cells. Glutamine deprivation slightly increased ROS production in control conditions but HDAC5 depletion did not further increase it (Figures 9a and b). The GSH/GSSG was not significantly modulated in HDAC5-depleted cells cultured without glutamine (Figure 9c). However, ATP level was decreased in HDAC5-depleted cells upon glutamine interference (Figures 9d–f), suggesting glutamine mainly serves as a metabolic source to drive the TCA cycle for energy generation rather than for its antioxidative capacity.

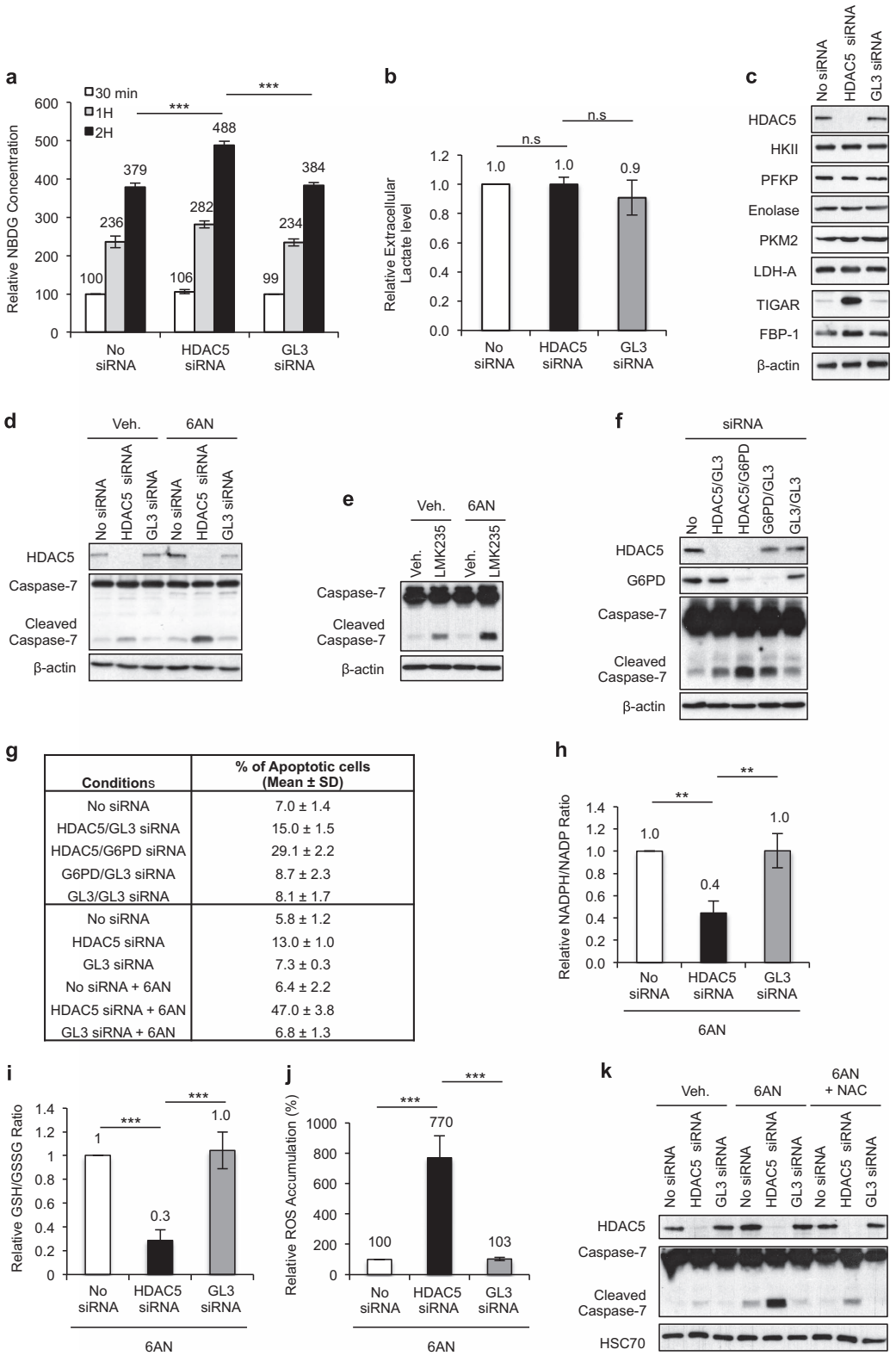

Finally, to demonstrate the *in vivo* relevance of glutamine interference and HDAC5 depletion, we looked at the effect of BPTES on the growth of HDAC5-depleted cells in mice. Administration of BPTES significantly reduced the growth of HDAC5-depleted cells *in vivo* (Figure 9g). Interestingly, combination of LMK235 or SAHA with BPTES caused similar effects as selective HDAC5 depletion both *in vitro* and *in vivo* (Figure 9h and Supplementary Figures S5A–G), demonstrating the clinical potential of combining such pharmacological molecules for therapeutic approach.

DISCUSSION

In cancer therapy, numerous HDACi have been tested in human clinical trials and some of them are FDA approved for haematological disorders. However, these molecules have demonstrated limited clinical benefit in solid tumours as single agents but they are generally more potent when combined with other chemotherapeutics, prompting the investigation of novel treatment combinations. The importance of individual HDAC inhibition for the observed antitumour activity is also extensively studied today. In addition, by defining the role of individual HDAC in molecular pathways, it helps to design appropriate therapeutic combinations targeting those pathways. Through this study, we are able to propose original combined strategies using specific HDAC5 inhibition and various metabolic inhibitors.

HDAC5 inhibition induces ROS production that mediates oxidative stress. This increase in ROS, up to intolerable levels, leads to apoptotic cell death. Besides apoptosis, HDAC5 depletion also induces an autophagic programme called mitophagy, a 'self-eating' process whereby ROS-producing mitochondria are eliminated.[23] This mechanism would help cells to survive as inhibition of HDAC5 silencing-dependent autophagy accelerates apoptosis, supporting the rationale for further testing autophagy inhibitors in conjunction with HDAC5 inhibition as a new combined therapy as already reported for broad-spectrum HDACi.[24,25]

Modulation of VUDP-1/TBP2/thioredoxin expression, which consequently increases intracellular ROS, has been proposed as one of the mechanisms underlying HDACi-induced cell death.[26] In the context of HDAC5 depletion, the cellular source of ROS depends on a combination of different events. First, accessory subunits of the mitochondrial complex I, NDUFB5, NDUFS4 and NDUFAB1, are modulated in absence of HDAC5. Although the supernumerary subunits were considered not to be essential for structure and function of mitochondrial complex I, it is now proposed that these subunits assist in complex I biogenesis and support the structural stability of complex I.[27] Therefore, deregulation of complex I organization might be responsible for excessive mitochondrial ROS formation observed in HDAC5-depleted cells. Second, our transcriptomic also reveals that HDAC5 depletion negatively modulates the expression of several antioxidant metal-chelating proteins that attenuates metal-dependent generation of ROS. Indeed, HDAC5 inhibition downregulates the expression of iron chelators such as ferritin. Therefore, the consequent increase of intracellular labile ferrous iron pool accentuates ROS production through Fenton reaction and further sensitizes HDAC5-depleted cells to cisplatin-based oxidative stress[27–30] (Figure 10a). This loss of ferritin expression in HDAC5-depleted cells also impairs the ability of those cells to chelate exogenous supply of ferrous iron, ultimately leading to oxidative stress driven by non-chelated iron. This also suggests that supplementation with iron should be considered as a suitable approach for developing novel combined treatments with HDAC5 inhibitor as demonstrated for other chemotherapeutic molecules.[31,32]

How HDAC5 is controlling gene expression is currently addressed. Changes in mRNA stability are one of the mechanisms underlying HDAC5 silencing-dependent decreases in mRNA expression. Indeed, our preliminary findings show that the half-life of some the most downregulated transcripts (for example NDUFB5, FTH1, stathmin and MTE1) were significantly decreased following HDAC5 depletion (unpublished data, ongoing study). Among the different class II HDAC, HDAC5 appears to be a specific regulator of this subset of genes, which are involved in iron-dependent management of oxidative stress response. This specific gene modulation in HDAC5-depleted cells probably explains why iron-dependent ROS production was not observed upon depletion of the other class II HDAC.

Attention has been paid to the intimate connection between cellular metabolism and redox homeostasis of cancer cells, with a particular emphasis on the role of glycolysis and glutaminolysis. By redirecting energetic substrates such as glucose and glutamine into the biochemical pathways that generate key antioxidant molecules, cancer cells can directly support the mechanisms of ROS detoxification.[19]

Therefore, identification of metabolic adaptive processes in HDAC5-depleted cancer cells could lead to the development of an effective therapeutic strategy aimed at disrupting this functional crosstalk and elevating the burden of oxidative stress. Here, we demonstrated that selective HDAC5 depletion leads to a metabolic survival adaptation towards glucose and glutamine catabolism. These two main nutrients seem to play complementary roles in promoting survival of HDAC5-depleted cells, where (i) glucose feeds the PPP pathway responsible for NADPH production and ROS detoxification; (ii) glutamine being imported at high rates to refill TCA cycle intermediates used for the continued maintenance of oxidative phosphorylation necessary to sustain energy supply

Figure 5. Reliance of HDAC5-depleted cells to PPP for cell survival. (**a**) Transfected HeLa cells were treated with 2-NBDG (20 μM) for 30 min – 1 h – 2 h, collected and analysed by flow cytometry. Results are presented as relative values arbitrarily fixed as 100% in No siRNA condition. Data are mean ± s.d. of three independent experiments. (**b**) Measure of extracellular lactate from transfected HeLa cells by nuclear magnetic resonance. Results are presented as a relative abundance of lactate arbitrarily fixed as 1 in No siRNA condition. Data are mean ± s.d. of three independent experiments carried out in triplicate. (**c**) Total protein extracts from transfected HeLa cells were processed for immunoblots with indicated antibodies. (**d**) Transfected HeLa cells were treated with 6-aminonicotinamide (6AN–10 μM) for additional 24 h. Immunoblots were performed with indicated antibodies. (**e**) LMK235 (1 μM)-treated HeLa cells were co-treated with 6-aminonicotinamide (6AN–10 μM). Immunoblots were performed with indicated antibodies. (**f**) HeLa cells were co-transfected with HDAC5 siRNA and G6PD siRNA. Immunoblots were performed with indicated antibodies. (**g**) Quantification of apoptosis of transfected HeLa cells co-treated with 6-aminonicotinamide (6AN–10 μM) or G6PD siRNA. Values represented the mean ± s.d. of three independent experiments. (**h**) NADPH/NADP ratio measured in transfected HeLa cells treated with 6-aminonicotinamide (6AN–10 μM) for 24 h. Results are presented as in Figure 2b. Values represented the mean ± s.d. of three independent experiments. (**i**) Measure of both reduced (GSG) and oxidized glutathione (GSSG) level in transfected HeLa cells cultured in presence of 6-aminonicotinamide (6AN–10 μM). Results are presented as in Figure 2c. Values represented the mean ± s.d. of three independent experiments. (**j**) ROS production in transfected HeLa cells co-treated with 6-aminonicotinamide (6AN–10 μM). Results are presented as in Figure 2a. Values represented the mean ± s.d. of four independent experiments carried out in triplicate. (**k**) Transfected HeLa cells were co-treated with 6-aminonicotinamide (6AN–10 μM) in the presence or absence of NAC (15 mM). Immunoblots were performed with indicated antibodies.

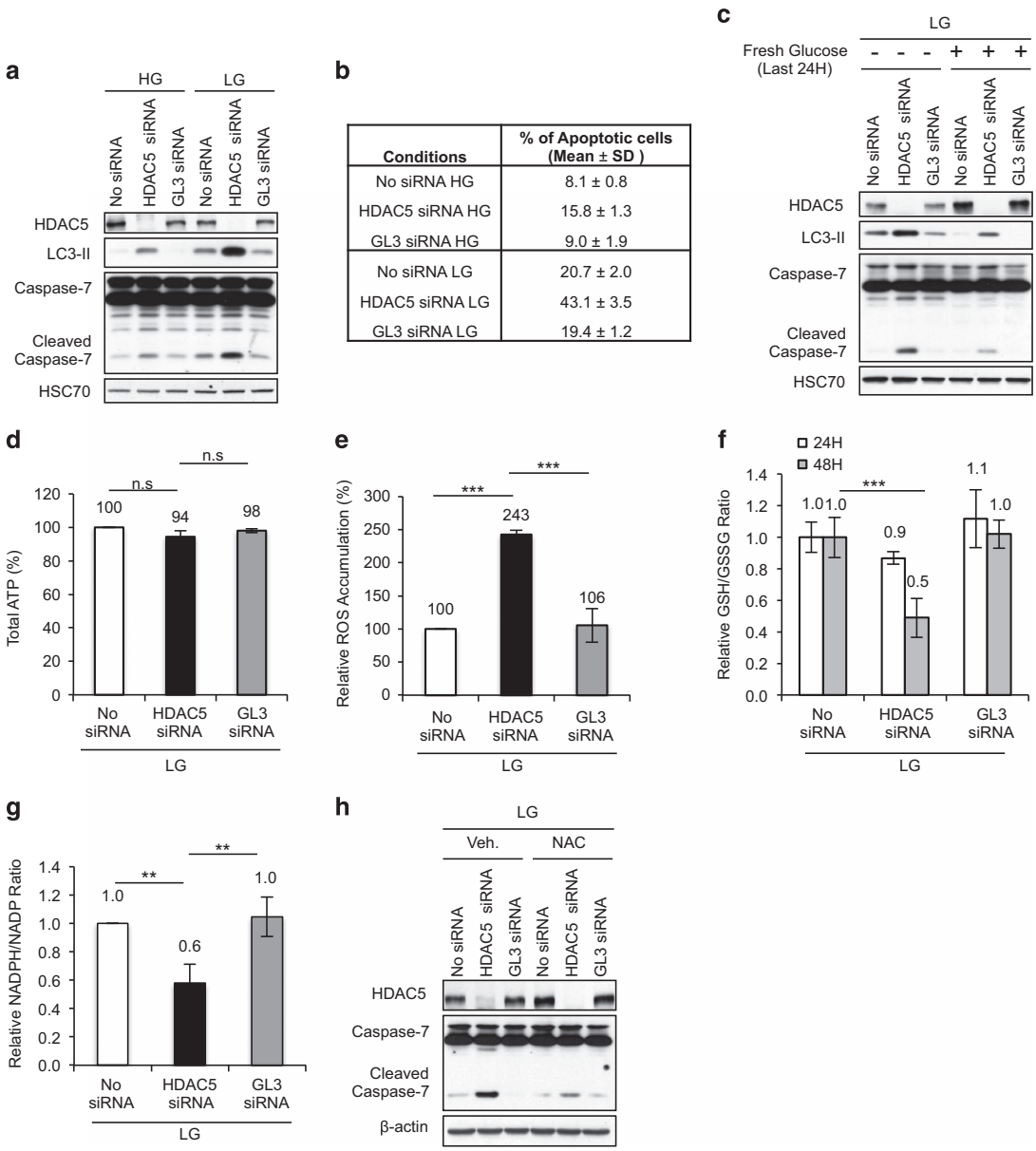

Figure 6. Glucose withdrawal increased apoptotic cell death of HDAC5-depleted cancer cells. (**a**) Transfected HeLa cells were cultured in high glucose (HG) or low glucose (LG) medium for an additional 48 h. Immunoblots were performed with indicated antibodies. (**b**) Quantification of apoptosis of transfected HeLa cells cultured in low glucose medium. Values represented the mean ± s.d. of three independent experiments. (**c**) Transfected HeLa were cultured in low glucose medium for 24 h and then supplemented with additional glucose (1 g/l) for additional 24 h. Immunoblots were performed with indicated antibodies. (**d**) Measure of total ATP levels in transfected HeLa cells cultured in low glucose medium for 48 h. Results are presented as in Figure 4c. Data are mean ± s.d. of three independent experiments carried out in triplicate. (**e**) ROS production in transfected HeLa cells cultured in low glucose medium for 48 h was quantified using DCFDA dye (5 μM) and flow cytometry. Results are presented as in Figure 2a. Data are mean ± s.d. of four independent experiments carried out in triplicate. (**f**) Measure of both reduced (GSG) and oxidized glutathione (GSSG) level in transfected HeLa cells cultured in low glucose medium for 24 and 48 h. Results are presented as in Figure 2c. Values represented the mean ± s.d. of three independent experiments. (**g**) NADPH/NADP ratio measured in transfected HeLa cells cultured in low glucose medium. Results are presented as in Figure 2b. Values represented the mean ± s.d. of three independent experiments. (**h**) Transfected HeLa cells were cultured in low glucose medium for 48 h in the presence of NAC (15 mM)). Immunoblots were performed with indicated antibodies.

(Figure 10b). The importance for aspartate metabolite in addition to alpha-ketoglutarate for survival of HDAC5-depleted cells is quite interesting. The role of this amino acid and its interaction with glutamine/glutamate and TCA cycle metabolism is becoming more and more studied in cancer cells[33–36] and this should be also further addressed in the context of HDAC5 depletion.

The systematic approach targeting glucose or glutamine-dependent metabolic pathways through clinically used metabolic drugs sensitizes HDAC5-depleted cancer cells to death. From the clinical point of view, the similar effect observed with LMK235, an inhibitor of HDAC5 activity, can lead to propose to clinicians to test this LMK235 molecule in combination with metabolic inhibitors as a new therapeutic strategy for cancer patients.

It is worth noting that redox mechanism and mechanism of adaptation/tolerance against ROS are rather complicated and dependent on specific cellular context. At the level of metabolism, multiple TCA cycle enzymes (for example IDH1, IDH2, SDH, FH)

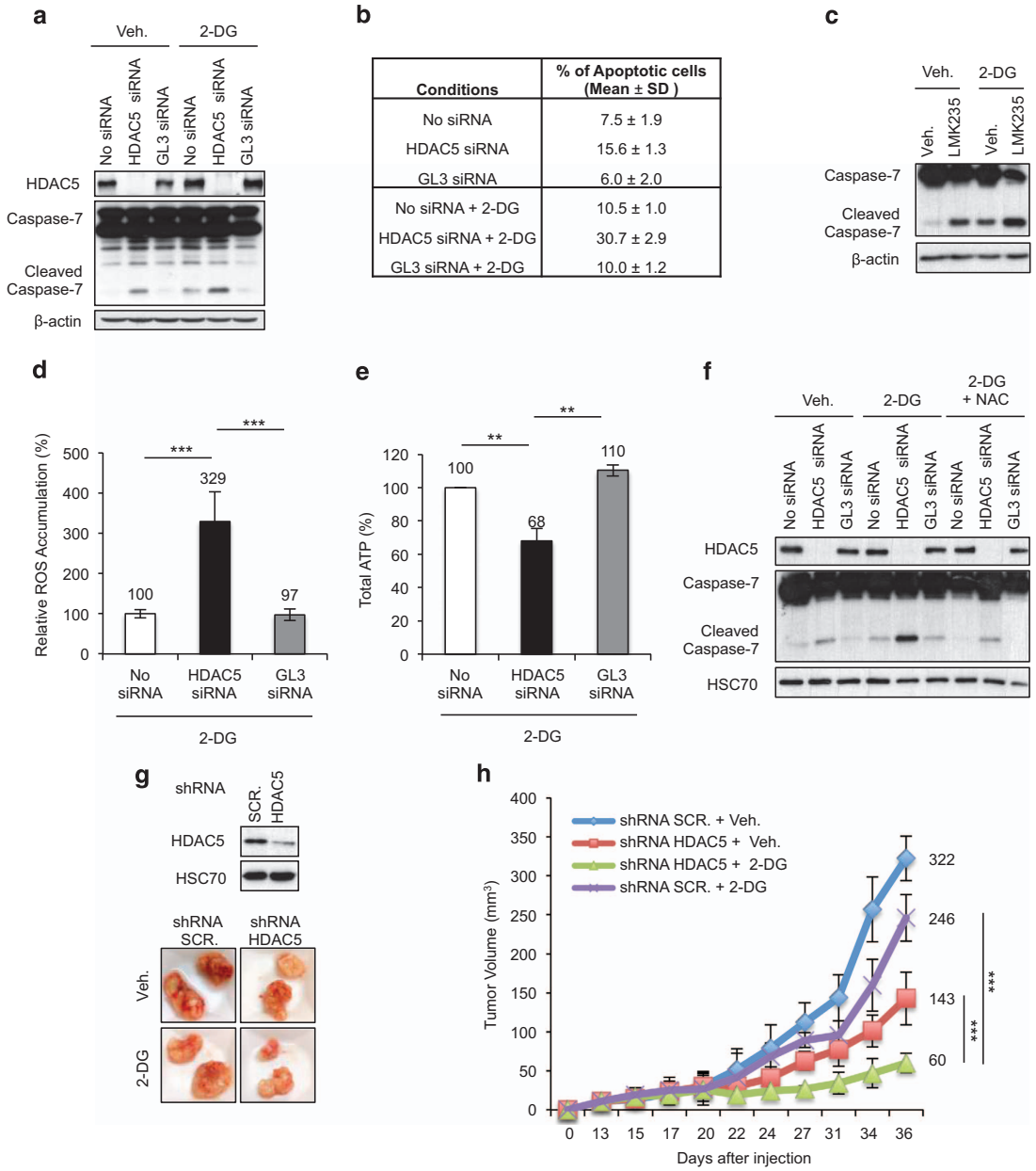

Figure 7. Glucose withdrawal in HDAC5-depleted cancer cells caused an oxidative stress. (**a**) Transfected HeLa cells were cultured in high glucose medium in presence of 2-deoxyglucose (2-DG–5 mM). Immunoblots were performed with indicated antibodies. (**b**) Quantification of apoptosis of transfected HeLa cells co-treated with 2-deoxyglucose (2-DG–5 mM). Values represented the mean ± s.d. of three independent experiments. (**c**) LMK235 (1 μM)-treated HeLa cells were co-treated with 2-deoxyglucose (2-DG–5 mM). Immunoblots were performed with indicated antibodies. (**d**) ROS production in transfected HeLa cells co-treated with 2-deoxyglucose (2-DG–5 mM). Results are presented as in Figure 2a. Data are mean ± s.d. of four independent experiments carried out in triplicate. (**e**) Measure of total ATP levels in transfected HeLa cells co-treated with 2-deoxyglucose (2-DG–5 mM). Results are expressed as in Figure 4c. Data are mean ± s.d. of three independent experiments carried out in triplicate. (**f**) Transfected HeLa cells were co-treated with 2-deoxyglucose (2-DG–5 mM) in presence or absence of NAC (15 mM). Immunoblots were performed with indicated antibodies. (**g**) Efficiency of HDAC5 shRNA was evaluated by immunoblots (*upper panel*). Representative pictures of corresponding excised tumours 36 days after subcutaneous injection of HeLa shRNA Scr and HeLa shRNA HDAC5 into NOD-SCID mice treated every day with 2-DG (250 mg/kg) (*lower panel*). (**h**) Measure of tumour volumes over time after injection. Values are mean ± s.d. of at least 12 tumours in each group.

have been found to be mutated in tumour tissues.[37,38] A detailed understanding of the role of these oncogenic metabolic mutations on cancer cell metabolism adaptation in the context of HDAC5 depletion would help to identify the relevant metabolic pathway to target in different types of cancers. It is also evident that variability exists across different cancer cells in terms of nutrient uptake and utilization. Therefore, tumours may harbour different metabolic flexibility that allows for the utilization of different precursors or metabolic pathways as a means of adaptation to HDAC5 inhibition.

Finally, our findings of the role of HDAC5 in regulation of iron-dependent ROS homeostasis in cancer cells open potential explanations for the role and mechanism of action of HDAC5 in other pathological disorders such as cardiovascular and neurodegenerative diseases. Chang *et al* demonstrated that HDAC5 knockout mice develop cardiac hypertrophy with age in response

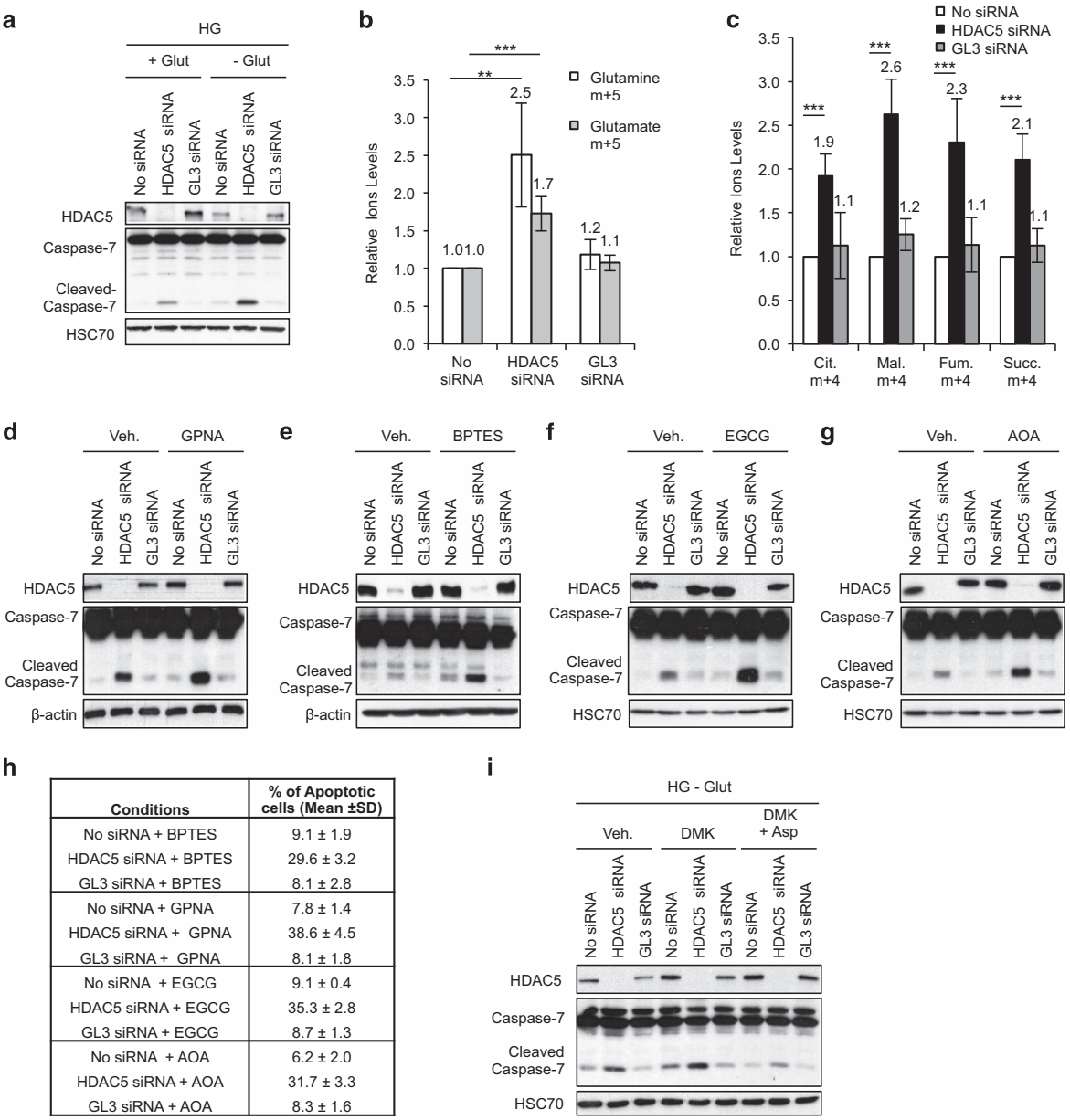

Conditions	% of Apoptotic cells (Mean ±SD)
No siRNA + BPTES	9.1 ± 1.9
HDAC5 siRNA + BPTES	29.6 ± 3.2
GL3 siRNA + BPTES	8.1 ± 2.8
No siRNA + GPNA	7.8 ± 1.4
HDAC5 siRNA + GPNA	38.6 ± 4.5
GL3 siRNA + GPNA	8.1 ± 1.8
No siRNA + EGCG	9.1 ± 0.4
HDAC5 siRNA + EGCG	35.3 ± 2.8
GL3 siRNA + EGCG	8.7 ± 1.3
No siRNA + AOA	6.2 ± 2.0
HDAC5 siRNA + AOA	31.7 ± 3.3
GL3 siRNA + AOA	8.3 ± 1.6

Figure 8. Glutamine importance in HDAC5-depleted cells. (**a**) Transfected HeLa cells were cultured in high glucose medium (HG) with (+Glut) or without glutamine (− Glut). Immunoblots were performed with indicated antibodies. (**b**, **c**) Transfected HeLa were cultured in high glucose medium for 24 h and then supplemented with fresh high glucose medium containing labelled [U-$^{13}C_5$]-glutamine for 8 h before metabolite extraction and GC/MS analysis. Results are presented as relative ion levels arbitrarily fixed as 1 in No siRNA condition. Values represented the mean ± s.d. of three independent experiments. (**d**–**g**) Transfected HeLa cells were treated with GPNA (500 μM) (**d**), BPTES (5 μM) (**e**), EGCG (10 μM) (**f**) or AOA (500 μM) (**g**). Immunoblots were performed with indicated antibodies. (**h**) Quantification of apoptosis of transfected HeLa cells co-treated with these different drugs. Values represented the mean ± s.d. of three independent experiments. (**j**) Transfected HeLa cells were cultured in glutamine-free medium supplemented or not with additional DMK (5 mM) alone or in combination with aspartate (Asp–5 mM). Immunoblots were performed with indicated antibodies.

to pressure overload and calcineurin signalling.[39] Our data open the possibility that alterations of metal metabolism and redox regulatory mechanisms operating in HDAC5-depleted cardiac cells might be a critical link between pressure overload and cardiac hypertrophy.[40] As reported by Agis-Balboa *et al*, loss of HDAC5 might be involved in Alzheimer disease,[41] a pathology that is often associated with disregulation of metal homeostasis and oxidative stress.[42–46] Similarly, metal regulation has been proposed as being a critical link between oxidative stress and ageing leading us to hypothesize that deregulation of HDAC5 might be a key mechanism in the free-radical and mitochondrial theories of ageing.

MATERIALS AND METHODS

Cells

Cancer cells were obtained from ATCC and were maintained in DMEM with 10% heat-inactivated foetal bovine serum. WI-38 cell line was obtained from the European Collection of Authenticated Cell Cultures (*ECACC*) and was maintained in minimum essential medium (Gibco, Merelbeke, Belgium) containing 5.5 mM glucose and supplemented with 2 mM L-Glutamine (Lonza), 100X MEN-non essential amino acids (Gibco) and 10% heat-inactivated foetal bovine serum (Gibco).

siRNA transfection

siRNAs were synthesized either by Eurogentec (Liège, Belgium) or Dharmacon (Lafayette, CO, USA) and transfected as previously described.[47]

Mock-transfected cells (No siRNA) or transfected with an irrelevant siRNA directed GL3 luciferase (GL3 siRNA) were used as negative controls. HDAC5 siRNA#1 are used unless indicated. siRNAs sequences are available.

Quantitative RT-PCR

Quantitative real-time PCR was performed as previously described.[48]

Immunofluorescence

Immunofluorescence was performed as described in Peixoto *et al.*[9]

Western blot

Western blots were performed as described in Peixoto *et al.*[9] All western blots are representative of at least three independent experiments.

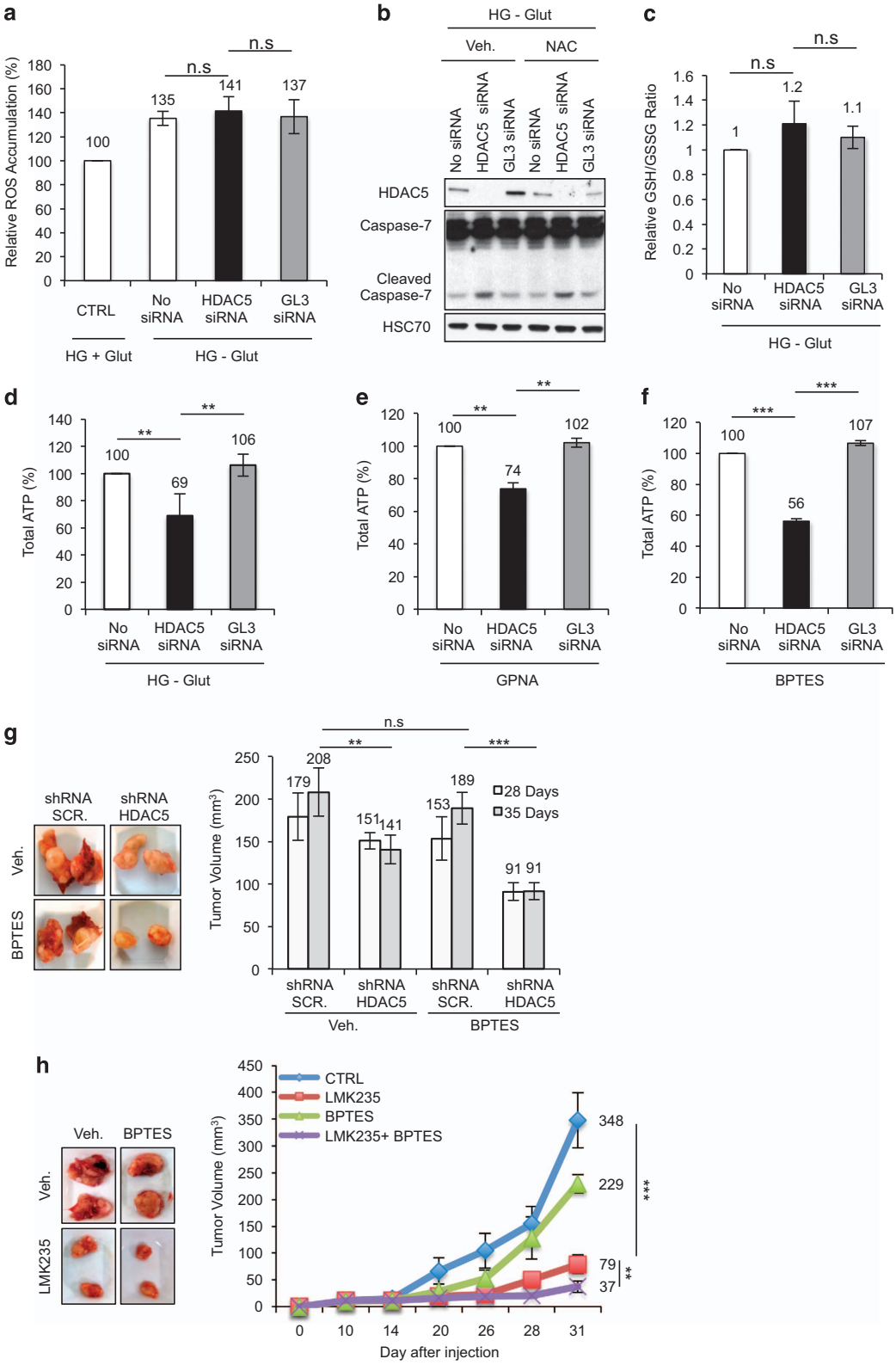

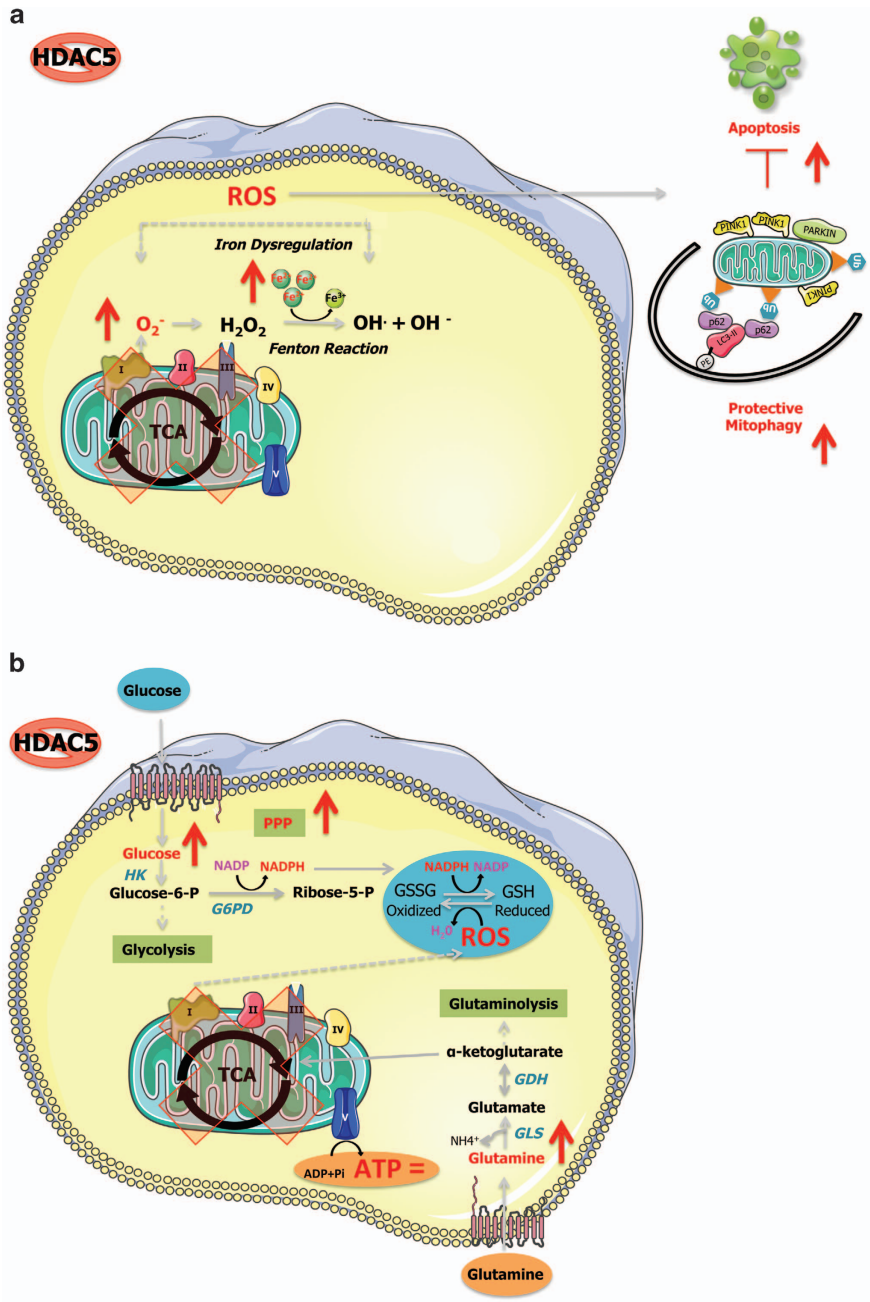

Figure 10. Schematic model illustrating the biological metabolic consequences of HDAC5 inhibition in cancer cells.

Figure 9. Glutamine withdrawal in HDAC5-depleted cancer cells caused a bioenergetic stress. (**a**) ROS production in transfected HeLa cells cultured without glutamine (– Glut) for 48 h was quantified using DCFDA dye (5 μM) and flow cytometry. Results are presented as in Figure 2a. Data are mean ± s.d. of four independent experiments carried out in triplicate. (**b**) Transfected HeLa cells were cultured in high glucose medium (HG) without glutamine (– Glut) but in the presence of NAC (15 mM). Immunoblots were performed with indicated antibodies. (**c**) Measure of both reduced (GSG) and oxidized glutathione (GSSG) level in transfected HeLa cells cultured as in (**a**). Results are presented as a relative ratio GSH/GSSG arbitrarily fixed as 1 in No siRNA condition. Values represented the mean ± s.d. and are representative of three independent experiments carried out in triplicate. (**d**–**f**) Measure of total ATP levels in transfected HeLa cells cultured in high glucose medium (HG) without glutamine (– Glut) for 48 h (**d**) or co-treated with GPNA (500 μM) (**e**) or BPTES (5 μM) (**f**). Results are expressed as in Figure 4c. Data are mean ± s.d. of three independent experiments carried out in triplicate. (**g**) *(Left panel)* Representative pictures of corresponding excised tumours 35 days after subcutaneous injection of HeLa shRNA Scr and HeLa shRNA HDAC5 into NOD-SCID mice daily treated with BPTES (10 mg/kg). *(Right panel)* Measure of tumour volumes 28 and 35 days after injection. Values are mean ± s.d. of at least 12 tumours in each group. (**h**) (*Left panel*) Representative pictures of corresponding excised tumours 31 days after subcutaneous injection of HeLa into NOD-SCID mice daily co-treated with BPTES (10 mg/kg) and LMK235 (40 mg/kg). (*Right panel*) Measure of tumour volumes over time. Values are mean ± s.d. of at least 12 tumours in each group.

ROS detection

ROS production was measured using DCFDA (Abcam, Cambridge, UK), Mitosox (mitochondrial ROS) (Molecular Probes, Eugene, OR, USA) fluorescent probe according to manufacturer's instructions or by ethylene production from KMB oxidation as described in Deby-Dupont *et al.*[49]

Respiration measurement

Oxygen consumption rates were measured as previously reported.[50]

Iron measurement

Iron levels were measured using an iron colorimetric assay kit (BioVision, San Francisco, CA, USA) according to the manufacturer's instructions.

Measurement of ATP/ADP/AMP levels

Relative cellular ATP content was measured using the ATP-based CellTiter-Glo Luminescent Cell Viability kit (Promega, Leiden, Netherlands) according to the manufacturer's protocol. The absolute amounts of cellular ATP, ADP and AMP content were measured using the HPLC-MS method published in Gangolf *et al.*[51]

Apoptosis analysis

Apoptosis was measured with the FITC-Annexin V apoptosis Detection Kit I (BD Biosciences, Erembodegen, Belgium) according to manufacturer's instructions.

Glucose uptake

Gluose uptake was followed using 2-NBDG (20 μM) according to supplier's instructions (Life Technologies, Carlsbad, CA, USA).

Mitochondria enrichment

Cells were washed once with cold PBS, trypsinized and resuspended in washing buffer (250 mM sucrose, 1 mM EDTA, 10 mM TRIS, pH 7.4). Cells were then centrifuged for 5 min at 94 × g and resuspended in homogeneization buffer (250 mM sucrose, 1 mM EDTA, 24 mM TRIS, pH 7.4) supplemented with protease inhibitors (complete EDTA free, Sigma-Aldrich, Overijse, Belgium) and 0.5 mg bovine serum albumin (Sigma-Aldrich). Physical cell breaking was performed using a glass/teflon tissue grinder and the cell lysate was centrifuged for 3 min at 685 × g. Resulting enriched-mitochondrial fraction was obtained after 3 min of centrifugation at 11992 × g.

Mitochondrial membrane potential

Mitochondrial membrane potential was determined with the fluorescent dye TMRE (Sigma-Aldrich). Cells were incubated with 2.5 nM TMRE for 30 min in PBS at 37 °C before flow cytometry analysis. As control, cells were treated with the uncoupling agent FCCP at 50 μM for 10 min before staining. Median fluorescence intensity values were corrected by FCCP background.

Measurement of reduced (GSH) and oxidized (GSSG) glutathione levels

GSH levels were measured using a fluorimetric assay kit (BioVision) according to the manufacturer's instructions.

Measurement of NADP and NADPH levels

NADP/NADPH levels were assessed fluorimetrically using an EnzyChrom $NADP^+$/NADPH assay kit (BioAssay Systems, Hayward, CA, USA) according to the manufacturer's instructions.

Nuclear magnetic resonance

Lactate production by nuclear magnetic resonance was performed as described in Sounni *et al.*[52]

Metabolite extraction and GC/MS analysis

Live cells were quenched with 90% methanol (Sigma-Aldrich). After 30 min incubation at − 80 °C, the extract was spun down at 14000 × g for 20 min at 4 °C. Supernatant was then allowed to complete evaporation on a 40 °C heated-block under nitrogen flow. 6.6 ng of internal standard myristic acid-D_{27} (Cambridge Isototope Laboratories, Tewksbury, MA, USA) dissolved in pyridine was added to each sample. 100 μl of 1:1 pyridine (Sigma-Aldrich) and MTBSTFA (Sigma-Aldrich) was added and derivatization was done at 60 °C for 60 min. GC/MS analysis was performed using TRACE™ Ultra Gas Chromatograph. The area under each peak was quantitated, inspected for accuracy, and normalized against total ion count, following which relative amounts were measured, setting metabolite amounts from No siRNA conditions to 1.

Human tumour xenograft

HeLa cells were injected subcutaneously into the two flanks of NOD-SCID immunodeficient mice (Charles River, Wilmington, MA, USA). Ten days after cell implantation, 24 mice bearing similar palpable tumour grafts (diameter of 15 mm^3) in each flank were randomly grouped into four groups with six mice in each group and then treated or co-treated daily by oral gavage with vehicle, BPTES (Sigma-Aldrich) (10 mg/kg/day), 2-DG (Sigma-Aldrich) (250 mg/kg/day) and/or SAHA (Selleckchem.com, Houston, TX, USA) (40 mg/kg/day) or LMK235 (Santa Cruz, Dallas, TX, USA) (40 mg/kg/day). Each drug was suspended in vehicle consisting of 0.5% carboxymethylcellulose, 1.8% NaCl, 0.4% Tween-80, 0.9% benzyl alcohol and ultrapure water adjusted to pH 6.0. Tumour growth was measured every 2 – 3 days and tumour volume was calculated according the following formula: length × $width^2 \times 0.52$. Caliper measurements were assessed in blind by multiple investigators. All animal procedures were approved by the Animal Welfare Committee of the University of Liège.

Statistical analysis

All experiments were carried out in, at least, biologic triplicates. Results were reported as means with their s.d. Statistical analysis was performed using one-way ANOVA or two-way ANOVA regarding the number of grouping factors. Group means were compared by a Bonferroni's post-test. Homoscedasticity (same variance) was assayed by a Levene's test. Normality (normal distribution) was assayed by the D'Agostino and Pearson test. All tests were performed with a 95% interval of confidence. n. s. not significant; * $P < 0.05$, ** $P < 0.01$, *** $P < 0.001$.

CONFLICT OF INTEREST

The authors declare no conflict of interest.

ACKNOWLEDGEMENTS

The authors thank the GIGA 'Cell Imaging and Flow Cytometry', the GIGA 'Transciptomic ' as well as the GIGA 'Animal' core facility for technical assistance. This work was supported by grants from the National Fund for Scientific Research (FNRS) (Belgium), TELEVIE, the Centre Anti-Cancéreux, Fonds Léon Frédéricq and Fonds Spéciaux de Recherche près de l'Université de Liège. PP and JC are FNRS-TELEVIE Post Doc. DM is a Research Associate. P DT is Senior Research Associate and LB is Research Director at the National Fund for Scientific Research (FNRS). CP, EH and AB are FNRS-TELEVIE fellows. NM is FRIA fellow.

AUTHOR CONTRIBUTIONS

Conception and design: E Hendrick, P Peixoto, A Blomme, D Mottet; Development of methodology: E Hendrick, P Peixoto, A Blomme, A Mouithys-Mickalad, D Serteyn, L Bettendorff, B Elmoualij, P De Tullio, G Eppe; Acquisition of data (provided animals, acquired and managed patients, provided facilities, etc): E Hendrick, P Peixoto, A Blomme, N Matheus, C Polese, J Cimino, A Frère, A Mouithys-Mickalad, P De Tullio, D Mottet; Analysis and interpretation of data (for example, statistical analysis, biostatistics, computational analysis): E Hendrick, P Peixoto, A Blomme, N Matheus, J Cimino, A Mouithys-Mickalad, P De Tullio, G Eppe, F Dequiedt, D Mottet; Writing, review, and/or revision of the manuscript: E Hendrick, P Peixoto, A Blomme, F Dequiedt, V Castronovo, D Mottet; Administrative, technical, or material support (that is, reporting or organizing data, constructing databases): E Hendrick, P Peixoto, A Blomme, N Matheus, C Polese, J Cimino, A Frère, G Eppe, D Mottet; Study supervision: E Hendrick, P Peixoto, V Castronovo, D Mottet.

REFERENCES

1 Mottet D, Castronovo V. Histone deacetylases: target enzymes for cancer therapy. *Clin Exp Metastasis* 2008; **25**: 183–189.
2 Nebbioso A, Carafa V, Benedetti R, Altucci L. Trials with 'epigenetic' drugs: an update. *Mol Oncol* 2012; **6**: 657–682.
3 Qiu T, Zhou L, Zhu W, Wang T, Wang J, Shu Y *et al.* Effects of treatment with histone deacetylase inhibitors in solid tumors: a review based on 30 clinical trials. *Future Oncol* 2013; **9**: 255–269.
4 Rangwala S, Zhang C, Duvic M. HDAC inhibitors for the treatment of cutaneous T-cell lymphomas. *Future Med Chem* 2012; **4**: 471–486.
5 Sawas A, Radeski D, O'Connor OA. Belinostat in patients with refractory or relapsed peripheral T-cell lymphoma: a perspective review. *Ther Adv Hematol* 2015; **6**: 202–208.
6 McDermott J, Jimeno A. Belinostat for the treatment of peripheral T-cell lymphomas. *Drugs Today (Barc)* 2014; **50**: 337–345.
7 Cheng T, Grasse L, Shah J, Chandra J. Panobinostat, a pan-histone deacetylase inhibitor: rationale for and application to treatment of multiple myeloma. *Drugs Today (Barc)* 2015; **51**: 491–504.
8 Thurn KT, Thomas S, Moore A, Munster PN. Rational therapeutic combinations with histone deacetylase inhibitors for the treatment of cancer. *Future Oncol* 2011; **7**: 263–283.
9 Peixoto P, Castronovo V, Matheus N, Polese C, Peulen O, Gonzalez a *et al.* HDAC5 is required for maintenance of pericentric heterochromatin, and controls cell-cycle progression and survival of human cancer cells. *Cell Death Differ* 2012; **19**: 1239–1252.
10 Fan J, Lou B, Chen W, Zhang J, Lin S, Lv F *et al.* Down-regulation of HDAC5 inhibits growth of human hepatocellular carcinoma by induction of apoptosis and cell cycle arrest. *Tumour Biol* 2014; **35**: 11523–11532.
11 He P, Liang J, Shao T, Guo Y, Hou Y, Li Y. HDAC5 promotes colorectal cancer cell proliferation by up-regulating DLL4 expression. *Int J Clin Exp Med* 2015; **8**: 6510–6516.
12 Liu Q, Zheng J-M, Chen J-K, Yan X-L, Chen H-M, Nong W-X *et al.* Histone deacetylase 5 promotes the proliferation of glioma cells by upregulation of Notch 1. *Mol Med Rep* 2014; **10**: 2045–2050.
13 Liu J, Gu J, Feng Z, Yang Y, Zhu N, Lu W *et al.* Both HDAC5 and HDAC6 are required for the proliferation and metastasis of melanoma cells. *J Transl Med* 2016; **14**: 7.
14 Zhang L, Wang K, Lei Y, Li Q, Nice EC, Huang C. Redox signaling: potential arbitrator of autophagy and apoptosis in therapeutic response. *Free Radic Biol Med* 2015; **89**: 452–465.
15 Urbich C, Rössig L, Kaluza D, Potente M, Boeckel J-N, Knau A *et al.* HDAC5 is a repressor of angiogenesis and determines the angiogenic gene expression pattern of endothelial cells. *Blood* 2009; **113**: 5669–5679.
16 Held NM, Houtkooper RH. Mitochondrial quality control pathways as determinants of metabolic health. *BioEssays* 2015; **37**: 867–876.
17 Baliga R, Zhang Z, Baliga M, Ueda N, Shah SV. In vitro and in vivo evidence suggesting a role for iron in cisplatin-induced nephrotoxicity. *Kidney Int* 1998; **53**: 394–401.
18 Ma P, Xiao H, Yu C, Liu J, Cheng Z, Song H *et al.* Enhanced cisplatin chemotherapy by iron oxide nanocarrier-mediated generation of highly toxic reactive oxygen species. *Nano Lett* 2017; **17**: 928–937.
19 Harris IS, Brugge JS. Cancer: the enemy of my enemy is my friend. *Nature* 2015; **527**: 170–171.
20 Mailloux RJ, Harper M-E. Uncoupling proteins and the control of mitochondrial reactive oxygen species production. *Free Radic Biol Med* 2011; **51**: 1106–1115.
21 Porporato PE, Dhup S, Dadhich RK, Copetti T, Sonveaux P. Anticancer targets in the glycolytic metabolism of tumors: a comprehensive review. *Front Pharmacol* 2011; **2**: 49.
22 Zhao Y, Butler EB, Tan M. Targeting cellular metabolism to improve cancer therapeutics. *Cell Death Dis* 2013; **4**: e532.
23 Kurihara Y, Kanki T, Aoki Y, Hirota Y, Saigusa T, Uchiumi T *et al.* Mitophagy plays an essential role in reducing mitochondrial production of reactive oxygen species and mutation of mitochondrial DNA by maintaining mitochondrial quantity and quality in yeast. *J Biol Chem* 2012; **287**: 3265–3272.
24 Gammoh N, Marks PA, Jiang X. Curbing autophagy and histone deacetylases to kill cancer cells. *Autophagy* 2012; **8**: 1521–1522.
25 Yang ZJ, Chee CE, Huang S, Sinicrope FA. The role of autophagy in cancer: therapeutic implications. *Mol Cancer Ther* 2011; **10**: 1533–1541.
26 Ahrens TD, Timme S, Ostendorp J, Bogatyreva L, Hoeppner J, Hopt UT *et al.* Response of esophageal cancer cells to epigenetic inhibitors is mediated via altered thioredoxin activity. *Lab Invest* 2016; **96**: 307–316.
27 Lenaz G, Baracca A, Barbero G, Bergamini C, Dalmonte ME, Del Sole M *et al.* Mitochondrial respiratory chain super-complex I-III in physiology and pathology. *Biochim Biophys Acta* 2010; **1797**: 633–640.
28 Chekhun VF, Lukyanova NY, Burlaka AP, Bezdenezhnykh NA, Shpyleva SI, Tryndyak VP *et al.* Iron metabolism disturbances in the MCF-7 human breast cancer cells with acquired resistance to doxorubicin and cisplatin. *Int J Oncol* 2013; **43**: 1481–1486.
29 Buranrat B, Connor JR. Cytoprotective effects of ferritin on doxorubicin-induced breast cancer cell death. *Oncol Rep* 2015; **34**: 2790–2796.
30 Shpyleva SI, Tryndyak VP, Kovalchuk O, Starlard-Davenport A, Chekhun VF, Beland FA *et al.* Role of ferritin alterations in human breast cancer cells. *Breast Cancer Res Treat* 2011; **126**: 63–71.
31 Arriaga JM, Greco A, Mordoh J, Bianchini M. Metallothionein 1G and zinc sensitize human colorectal cancer cells to chemotherapy. *Mol Cancer Ther* 2014; **13**: 1369–1381.
32 Margalit O, Simon AJ, Yakubov E, Puca R, Yosepovich A, Avivi C *et al.* Zinc supplementation augments in vivo antitumor effect of chemotherapy by restoring p53 function. *Int J Cancer* 2012; **131**: E562–E568.
33 Birsoy K, Wang T, Chen WW, Freinkman E, Abu-Remaileh M, Sabatini DM. An essential role of the mitochondrial electron transport chain in cell proliferation is to enable aspartate synthesis. *Cell* 2015; **162**: 540–551.
34 Allen EL, Ulanet DB, Pirman D, Mahoney CE, Coco J, Si Y *et al.* Differential aspartate usage identifies a subset of cancer cells particularly dependent on OGDH. *Cell Rep* 2016; **17**: 876–890.
35 Patel D, Menon D, Bernfeld E, Mroz V, Kalan S, Loayza D *et al.* Aspartate rescues S-phase arrest caused by suppression of lutamine utilization in KRas-driven cancer cells. *J Biol Chem* 2016; **291**: 9322–9329.
36 Ratnikov B, Aza-Blanc P, Ronai ZA, Smith JW, Osterman AL, Scott DA. Glutamate and asparagine cataplerosis underlie glutamine addiction in melanoma. *Oncotarget* 2015; **6**: 7379–7389.
37 Jang M, Kim SS, Lee J. Cancer cell metabolism: implications for therapeutic targets. *Exp Mol Med* 2013; **45**: e45.
38 Gaude E, Frezza C. Defects in mitochondrial metabolism and cancer. *Cancer Metab* 2014; **2**: 10.
39 Chang S, McKinsey TA, Zhang CL, Richardson JA, Hill JA, Olson EN. Histone deacetylases 5 and 9 govern responsiveness of the heart to a subset of stress signals and play redundant roles in heart development. *Mol Cell Biol* 2004; **24**: 8467–8476.
40 Sag CM, Santos CXC, Shah AM. Redox regulation of cardiac hypertrophy. *J Mol Cell Cardiol* 2014; **73**: 103–111.
41 Agis-Balboa RC, Pavelka Z, Kerimoglu C, Fischer A. Loss of HDAC5 impairs memory function: implications for Alzheimer's disease. *J Alzheimers Dis* 2013; **33**: 35–44.
42 Zhu X, Su B, Wang X, Smith MA, Perry G. Causes of oxidative stress in Alzheimer disease. *Cell Mol Life Sci* 2007; **64**: 2202–2210.
43 McCord MC, Aizenman E. The role of intracellular zinc release in aging, oxidative stress, and Alzheimer's disease. *Front Aging Neurosci* 2014; **6**: 77.
44 Altamura S, Muckenthaler MU. Iron toxicity in diseases of aging: Alzheimer's disease, Parkinson's disease and atherosclerosis. *J Alzheimers Dis* 2009; **16**: 879–895.
45 Di Domenico F, Barone E, Perluigi M, Butterfield DA. Strategy to reduce free radical species in Alzheimer's disease: an update of selected antioxidants. *Expert Rev Neurother* 2015; **15**: 19–40.
46 Grünblatt E, Bartl J, Riederer P. The link between iron, metabolic syndrome, and Alzheimer's disease. *J Neural Transm* 2011; **118**: 371–379.
47 Mottet D, Bellahcène A, Pirotte S, Waltregny D, Deroanne C, Lamour V *et al.* Histone deacetylase 7 silencing alters endothelial cell migration, a key step in angiogenesis. *Circ Res* 2007; **101**: 1237–1246.
48 Mottet D, Pirotte S, Lamour V, Hagedorn M, Javerzat S, Bikfalvi A *et al.* HDAC4 represses p21(WAF1/Cip1) expression in human cancer cells through a Sp1-dependent, p53-independent mechanism. *Oncogene* 2009; **28**: 243–256.
49 Deby-Dupont G, Mouithys-Mickalad A, Serteyn D, Lamy M, Deby C. Resveratrol and curcumin reduce the respiratory burst of Chlamydia-primed THP-1 cells. *Biochem Biophys Res Commun* 2005; **333**: 21–27.
50 Ceusters JD, Mouithys-Mickalad AA, Franck TJ, Derochette S, Vanderplasschen A, Deby-Dupont GP *et al.* Effect of myeloperoxidase and anoxia/reoxygenation on mitochondrial respiratory function of cultured primary equine skeletal myoblasts. *Mitochondrion* 2013; **13**: 410–416.
51 Gangolf M, Czerniecki J, Radermecker M, Detry O, Nisolle M, Jouan C *et al.* Thiamine status in humans and content of phosphorylated thiamine derivatives in biopsies and cultured cells. *PLoS One* 2010; **5**: e13616.
52 Sounni NE, Cimino J, Blacher S, Primac I, Truong A, Mazzucchelli G *et al.* Blocking lipid synthesis overcomes tumor regrowth and metastasis after antiangiogenic therapy withdrawal. *Cell Metab* 2014; **20**: 280–294.

Supplementary Information accompanies this paper on the Oncogene website (http://www.nature.com/onc)